Transplantable human thyroid organoids generated from embryonic stem cells to rescue hypothyroidism

Mírian Romitti [1], Barbara de Faria da Fonseca [1], Gilles Doumont [2], Pierre Gillotay [1], Adrien Tourneur [1], Sema Elif Eski [1], Gaetan Van Simaeys [2,3], Laura Chomette [1], Helene Lasolle [1], Olivier Monestier [1], Dominika Figini Kasprzyk [1], Vincent Detours [1], Sumeet Pal Singh [1], Serge Goldman [2,3], Samuel Refetoff [4] and Sabine Costagliola [1]

[1] Institut de Recherche Interdisciplinaire en Biologie Humaine et Moléculaire (IRIBHM), Université Libre de Bruxelles (ULB), Brussels, Belgium

[2] Center for Microscopy and Molecular Imaging (CMMI), Université libre de Bruxelles (ULB), Charleroi (Gosselies), Belgium

[3] Service de Médecine Nucléaire, Hôpital Érasme, Université libre de Bruxelles (ULB), Brussels, Belgium

[4] Departments of Medicine, Pediatrics and Committee on Genetics, The University of Chicago, Chicago, IL, USA

The function of the thyroid gland is to capture iodide in order to synthesize hormones that act on almost all tissues and are essential for normal growth and metabolism. Low plasma levels of thyroid hormones lead to hypothyroidism, which is one of the most common disorder in humans which is not always satisfactorily treated by lifelong hormone replacement. Therefore, in addition to the lack of *in vitro* tractable models to study human thyroid development, differentiation and maturation, there is a need for new therapeutic approaches that involve replacement of thyroid tissue responsive to changing demands for thyroid hormone. Here we report the first transplantable thyroid

organoids derived from human embryonic stem cells capable of restoring plasma thyroid hormone to athyreotic mice as a proof of concept for future therapeutic development.

Hypothyroidism is a very common disorder with a prevalence of 1% to 5% worldwide. It results from insufficient thyroid hormone (TH) production due to autoimmune damage to the thyroid gland, iodide excess or deficiency, external irradiation, genetic defects or other defects manifesting at birth (congenital hypothyroidism, CH) and surgical or radioactive thyroid ablation to treat hyperthyroidism or thyroid cancer [1–3]. Despite well-established TH replacement therapy, it is estimated that up to one-third of patients do not receive an adequate treatment [4,5] while a large proportion have impaired health-related quality of life, particularly psychological well-being [6,7]. In addition, studies have shown that children with CH can develop motor, cognitive, and social dysfunction even when diagnosed through newborn screening followed by early institution of TH replacement [7,8]. Indeed, constant exogenous supply of TH does not provide for changes in TH requirement associated with growth, puberty, pregnancy and stress, leaving room for new therapeutic approaches, such as regenerative medicine, that would accommodate the variation in TH demand.

In recent years, significant progress has been made in the development and application of human cell-based models for the study of human biology and disease modeling. Human embryonic stem cell (ESC)-based protocols have been developed and led to the generation of several types of human organoids that include brain, intestine, stomach, liver, kidney, lung, endometrium, prostate, pancreas, and retina [8,9]. With regard to the thyroid, murine ESC-derived organoids have been shown to recapitulate *in vitro* the developmental stages of the thyroid gland with the ability to produce TH *in vitro* and *in vivo* after transplantation to mice with ablated thyroid glands [11–15].

50 In contrast, human thyroid cells so far generated from stem cells have not shown full maturation
51 *in vitro* and ability to compensate for low TH levels when transplanted into animals devoid of
52 thyroid tissue [10–14]. These difficulties in producing functional human thyroid follicles capable
53 of restoring thyroid function *in vivo* have been partially overcome by using organoids generated
54 from suspensions of adult human thyroid cells, but with some limitations. Hence, Coppes et al.
55 [15] generated thyrospheres from human thyroid glands, but 26 weeks are required to detect
56 human thyroid tissue when these organoids are transplanted into hypothyroid mice, and plasma
57 levels of T4 did not increase significantly [15].
58 Given the lack of a functional *in vitro* thyroid model to further explore various aspects related
59 to thyroid development, maturation and disease and to provide an alternative to imperfect drug
60 treatment to restore thyroid function in patients, there is an urgent need to define an optimized
61 strategy to generate TH producing human follicles from stem cells. We used forward
62 programming by transient overexpression of *NKX2-1* and *PAX8* transcription factors (TFs) and
63 manipulation of signaling pathways in combination with stepwise transcriptomic
64 characterization, to generate a functional human thyroid from pluripotent stem cells that
65 recapitulates thyroid function *in vitro* and *in vivo*.
66
67 ***In vitro* differentiation of human thyroid cells**
68 <u>*hESC line generation and characterization:*</u> in recent years, mouse ESC-derived *in vitro*
69 thyroid models have provided understanding of mechanisms involved in thyroid development
70 and maturation [10,16–19]. However, replication of the protocols using hESC/iPSC was insufficient
71 to generate a functional human thyroid *in vitro* [14,16–18]. Since we have previously shown that
72 forward programming [20–23] by transient overexpression of the transcription factors, *Nkx2-1* and
73 *Pax8* [24] leads to high efficiency of thyroid differentiation and functional follicle formation from
74 mouse ESC [16], we used a similar approach to generate a recombinant human ESC line. First,

75 we took advantage of a previously generated NKX2-1$^{WT/GFP}$ knock-in hESC line [25] (Extended
76 data Fig. 1a) to track thyroid differentiation and cell organization using the NKX2-1^{GFP}
77 reporter. Furthermore, the hESC-NKX2-1$^{WT/GFP}$ line was modified to allow transient
78 expression of *NKX2-1* and *PAX8*, by adding doxycycline (Dox; 1 mg/ml; Extended data Fig.
79 1b) to the culture medium (Fig. 1a). The resulting hESCs, had normal karyotype and ability to
80 spontaneously differentiate into cells from the three germ layers (Extended data Fig. 1c-d,
81 respectively).
82 *Induction of thyroid status:* The modified hESCs were first grown for 2 days in hanging drops
83 to allow the formation of embryoid bodies (EBs) (Fig. 1a). The generated EBs were then
84 cultured in matrigel drops and endoderm was induced by adding Activin A for 3 days. This
85 treatment resulted in increased mRNA levels of the endoderm markers *SOX17* and *FOXA2*
86 (Extended data Fig. 1e) and simultaneously improved the percentage of FOXA2 + cells,
87 particularly in the inner compartment of EBs (Extended data Fig. 1f). After induction of the
88 endoderm, Dox treatment promoted the overexpression of *NKX2-1* and *PAX8*. After 4 days,
89 expression of NKX2-1 and PAX8 was detected by immunofluorescence in a large proportion
90 of Dox-treated cells but not in the absence of Dox (Extended data Fig. 1g). Furthermore, qPCR
91 analysis showed that not only were exogenous *NKX2-1* and *PAX8* gene expression levels
92 significantly upregulated, but endogenous *NKX2-1*, *PAX8*, *FOXE1*, *TG*, and *TSHR* mRNA
93 levels were also increased as early as day 9 (Extended data Fig. 1h). To determine whether
94 forced overexpression of thyroid TFs leads to autonomous activation of endogenous cell
95 programming in thyroid fate, Dox treatment was interrupted and cells were incubated in basal
96 differentiation medium for 7 days (from day 9 to day 16). qPCR analysis revealed that
97 exogenous *PAX8* expression at day 9 was similar to endogenous *PAX8* expression, but the
98 levels of exogenous TFs decreased over time and reached control levels (+AA -Dox) from day
99 12. In contrast, endogenous *PAX8* levels increased dramatically and reached a plateau from

100 day 14 (Extended data Fig. 1i). These results suggest that Dox induction of TFs the endogenous
101 transcriptional machinery is activated, initiating the thyroid differentiation program.
102 *Thyroid cell population expansion and early differentiation* were promoted by incubation with
103 8-br-cAMP for 2 weeks (from day 16 to day 30). Flow cytometry analysis confirmed growth
104 of the thyroid population resulting in approximately 25% of total cells expressing NKX2-1^{GFP}
105 at day 30 (Fig. 1b), reflecting the increase in proliferation as around 90% of NKX2-1^{GFP+} cells
106 continuously expressed KI67 during the treatment period (Extended data Fig. 2a). Accordingly,
107 transcriptomics analysis performed in NKX2-1^{GFP} cells showed high levels of various
108 proliferation markers (Extended data Fig. 2b). In parallel, an increase in expression of early
109 thyroid markers was also observed over time (+AA +Dox +cAMP), confirming the role of
110 cAMP in cell differentiation (Fig. 1c). This was accompanied by a steady expression of key
111 genes such as *NKX2-1*, *TG*, and *TSHR* from day 23 (Extended data Fig. 2c). However, key
112 maturation markers, such as *NIS*, *TPO* and *DUOX* family, were not significantly induced by
113 cAMP, suggesting that it is not sufficient to promote thyroid maturation and function. By
114 tracking NKX2-1^{GFP+} cells we observed at day 28, that thyroid cells start to form follicle-like
115 structures and immunostaining shows marked expression of *TG* and *PAX8*. Though, the cells
116 were not organized in single-layered follicles, but a luminal compartment was observed
117 (Extended data Fig. 2d), suggesting that the process of folliculogenesis is not yet complete at
118 this stage.
119 *Thyroid maturation and function:* since cAMP treatment was not able to fully promote thyroid
120 maturation despite significant expression of *TSHR*, we explored additional ways to promote
121 thyroid differentiation. As the TSHR controls more than the Gs regulatory cascade [26], we first
122 replaced cAMP with hrTSH from day 30. Second, we added dexamethasone (from day 30) and
123 the TGFβ inhibitor SB431542 (from day 37), based on transcriptomic data showing substantial
124 levels of TGFβ pathway markers (Extended data Fig. 2f) among NKX2-1 cells, and the known

125 inhibition of thyroid differentiation by inflammation and TGFβ pathway stimulation [27–31].
126 Together, these alterations of the protocol (Fig. 1a) resulted in significant improvement in the
127 expression of key thyroid maturation markers, including *TSHR, TG, NIS /SLC5A5, TPO, DIO2,*
128 and the *DUOX* family (Figs. 1c and Extended data Fig. 2e), while mRNA levels of TGFβ
129 pathway effectors were reduced, particularly receptors (Extended data Fig. 2f). Subsequently,
130 PAX8 and ZO -1 co-staining revealed monolayer-organized follicles with a well delimited
131 lumen (Extended data Fig. 2g). On the other hand, the proportion of NKX2-1+ cells was
132 maintained over time, whereas NKX2-1/KI67+ cells clearly decreased at day 47, compared to
133 the early time points (Fig. 1b and Extended data Fig. 2a, respectively). Of note, our human
134 hESC-derived protocol for thyroid generation follows the sequential events observed *in vivo*,
135 as in human, thyroid development takes approximately 40 days from specification to
136 folliculogenesis[32,33], a similar developmental time is required in our *in vitro* model.
137 Considering that we artificially induce thyroid progenitor cells formation by forcing the
138 expression of *NKX2-1* and *PAX8*, the expression of maturation genes follows the physiological
139 sequence, with *TG* and *TSHR* being the first detected genes, followed by *TPO* and *NIS /SLC5A5*
140 [32,33]. A similar effect trend was observed in thyroid population expansion, organization and
141 follicle formation. However, even though the TH machinery seems to be complete, we could
142 not detect TH-producing follicles at day 45.
143
144 **Single cell characterization of human thyroid organoids.**
145 To better characterize the resulting cell composition of our hESC-derived thyroid model,
146 scRNA-seq analyzes were performed at day 45. Since the efficiency of the present protocol is
147 approximately 25%, we enriched the proportion of NKX2-1^{GFP+} cells to 60%, the remaining
148 sorted cells belonging to the GFP- population. A total of approximately 6,000 cells were used
149 for scRNA-seq library preparation using the droplet-based assay from 10X Genomics. After

150 quality control (see extended data methods), we obtained 1874 cells that met all the criteria.
151 Among those cells, we identified 7 clusters (Fig. 1d-e), including a cluster of thyroid follicular
152 cells with 1176 cells showing expression of genes involved in development and function,
153 including *NKX2-1*, *PAX8*, *FOXE1*, *HHEX*, *TG*, *TSHR*, and *TPO* (Fig. 1e-f). Of note, we
154 identified three sub-clusters among the thyroid cells: Thyroid "progenitors" (477 cells)
155 expressing mainly the thyroid TFs; immature thyrocytes (365 cells) expressing also *TG* and
156 *TSHR*; and mature thyrocytes (334 cells) showing a canonical thyroid signature with a higher
157 proportion of *TPO*-expressing cells (Fig. 1e-f and Extended data Fig. 3a). Furthermore,
158 pseudotime analysis reveals a branch of differentiation originating from thyroid progenitors
159 and moving toward immature and progressive mature thyrocytes (Fig. 1g). This transition was
160 used to generate the trend of gene expression for the different thyroid markers along the
161 trajectory (Fig. 1h), which follows the expected dynamics, with TFs appearing first, followed
162 by *TSHR*, *TG*, and *TPO* expression (Fig. 1e).
163 The identity and molecular signature of the remaining cells was characterized, and we
164 identified four non-thyroidal clusters: fibroblasts (146 cells) expressing *DCN*, *COL1A2*, and
165 *PPRX1*; cardiovascular cells (182 cells) enriched in *ACTA2* and *TNNT2 markers*; airway cells
166 (203 cells) expressing *KRT5* and *TP63* and endoderm-epithelial cells (167) expressing *FOXA1*,
167 *FOXA2*, and *ADAM28* (Fig. 1d-e and Extended data Fig. 3b). Even if NKX2-1 also plays a
168 critical role in lung and forebrain development [34], our protocol predominantly generates thyroid
169 cells, since more than 75% of *NKX2-1*+ cells co-express *PAX8* and/or other thyroid markers.
170 *Connectome:* To predict possible crosstalk between thyroid cells and the other cells present in
171 the organoids, we used CellPhone- DB, to access the ligand-receptor interaction pairs identified
172 between thyroid clusters and other cell types. Interestingly, we found significant cell-cell
173 interactions between thyroid cells with mainly mesodermal cells associated with several
174 signaling pathways described as involved in thyroid development and physiology (Extended

175 data Fig. 3c). Previous studies performed *in vivo* and using stem cell-derived organoids have
176 described the critical role of BMP and FGF signaling pathways in regulating thyroid
177 specification, as well as how WNT signaling can influence thyroid development and determine
178 lineage choice toward lung specification [10,17,19,35,36]. Here, we observed that in our multicellular
179 organoid model, the presence of mesoderm-derived cells could be beneficial for thyroid
180 development without supplementation of factors, as we observed that fibroblasts and
181 cardiovascular cells are an important source of *BMP2*, *BMP4*, and *FGF2* ligands, whereas
182 thyroid cells express the specific receptors (Extended data Fig. 3c-d). In addition, insulin-like
183 growth factor (IGF-I) is known to support normal thyroid size and function, in part by
184 enhancing TSH sensitivity [37]. In addition to BMP and FGF, mesodermal, airway and endoderm
185 epithelial cells also provide significant amounts of *IGF-1* and *IGF-2*, while progenitors and
186 immature thyrocytes express *IGF1R* and mature thyrocytes mainly express *IGF2R*. On the
187 other hand, we also observed that fibroblasts and cardiovascular cells express significant
188 amounts of *WNT2*, *WNT5A*, *TGFb1*, and *TGFb2*, whereas thyroid cells express their respective
189 receptors (Extended data Fig. 3c-d). As described previously, in our model, inhibition of TGFβ
190 signaling leads to enhanced thyroid maturation, and this effect may also be related to repression
191 of such signals from mesodermal-like cells.
192
193 **Promotion of thyroid hormone synthesis**
194 Despite the cell differentiation and follicular organization at day 45, single-cell RNA profiling
195 revealed that a substantial proportion of the thyrocyte population was not fully mature, which
196 may explain the lack of TH detection at this stage. To promote functionality, we kept the
197 thyroid cells in culture for a longer period of time, mimicking the *in vivo* thyroid maturation.
198 *Complete in vitro human thyroid maturation and thyroid hormone synthesis:* Human thyroid
199 development begins around day 20 post fertilization, while completed organogenesis and TH

200 production can be detected at day 70 [32,33]. Based on the time required for thyroid full maturation
201 and TH synthesis *in vivo*, we kept the organoids growth for two additional weeks using the
202 same conditioned medium (Fig. 1a). Immunostaining revealed a large proportion of well-
203 organized follicles expressing NKX2-1, E-CADHERIN (Fig. 2a) and TG which accumulated
204 mainly in the lumen (Fig. 2b). In addition, marked TPO staining was observed in most follicular
205 structures, with accumulation at the apical membrane indicating an enhancement of maturation
206 (Fig. 2c). Finally, prolongation of the differentiation protocol resulted in TH synthesis, as
207 evidenced by the detection of T4 in the lumen of hESC-derived thyroid follicles (Fig. 2d).
208 *Assessment of in vivo functionality of hESC-derived thyroid follicles:* To evaluate the *in vivo*
209 functionality of hESC-derived thyroid follicles, the recovery of TH was measured in NOD-
210 SCID mice whose thyroid gland was ablated with radioactive iodine (RAI) following low-
211 iodine diet to enhance thyroidal RAI uptake. Thyroid ablation was confirmed after 4 weeks by
212 SPEC-CT imaging with ^{123}I. Organoids were harvested and filtered at day 45 to remove most
213 isolated cells and transplanted under the kidney capsule of mice with intact and ablated thyroid
214 glands (Fig. 3a). Due to technical problems caused by the radiosensitivity of immunodeficient
215 mice [38,39], 60% of the irradiated animals died during the experimental period. At the end of the
216 experiment, 6 non-transplanted and 4 transplanted mice had survived and could be compared
217 with 6 untreated animals that served as controls.
218 Histological evaluation of the renal region five weeks after transplantation showed successful
219 implantation of the transplanted organoids in the host niche (Fig. 3b). HE staining showed
220 numerous follicles organized in a manner characteristic of thyroid tissue (Fig. 3b and Extended
221 data Fig. 4a). The presence of blood vessels in close proximity to the thyroid follicles is
222 essential for the TH release and transport to target tissues. Indeed, blood vessels and stromal
223 cells could be observed in the vicinity of the thyroid follicles (Extended data Fig. 4a-b).
224 Immunostaining for the platelet-derived endothelial cell adhesion molecule CD31 revealed a

225 dense network of small blood vessels surrounding the thyroid follicles, demonstrating the
226 formation of classic angio-follicular units (Extended data Fig. 4b). The absence of staining
227 overlap between CD31 and Human Nuclear Antigen (HNA) provided unequivocal evidence
228 that the vessels originated from host cells (Extended data Fig. 4b). On the other hand, the
229 stromal cells were derived from the grafted cells since they co-expressed HNA and a-SMA
230 (Extended data Fig. 4c). HE staining showed that the derived follicular epithelium included
231 both active follicles, which appeared cuboidal to low columnar, and inactive ones, in which the
232 cells were squamous (Fig. 4d). Further immunohistochemical analysis supported the formation
233 of functional thyroid follicles (NKX2-1+) at the graft site, including cell polarization labeled
234 by E-Cadherin, TG cytosolic expression and deposition in the luminal compartment, and the
235 appearance of TPO in the cytoplasm and mainly at the apical membrane (Fig. 3c). The
236 transplanted tissue had a similar thyroid gene expression signature compared to human thyroid
237 tissue (Extended data Fig. 4e).
238 SPECT-CT imaging was used to track the human thyroid graft performance, by the ability of
239 NIS-dependent iodide uptake by thyroid tissue [40]. Images were acquired four weeks after
240 transplantation and showed a strong uptake signal in the neck (where the thyroid gland is
241 located) of non-ablated mice. In thyroid gland ablated transplanted mice, ^{123}I uptake was
242 markedly decreased in the neck, but a very strong signal was detectable at the site of
243 transplantation, near the kidney (Fig. 4a). ^{123}I quantification in SPECT images expressed as
244 percent injected dose (% ID [40]) confirmed the uptake capacity of the transplanted tissue, with
245 a % ID slightly lower compared to the thyroid tissue, while very low uptake values were
246 detected in the neck of the hypothyroid non-transplanted mice (1.66 (0.96-2.14); 2.40 (1.72-
247 4.91) and 0.010 (0.0023-0.032) % ID, respectively; $p<0.01$; Fig. 4a-b).
248 More importantly, transplanted animals presented a marked increase in plasma T4 levels (1.26
249 (0.86-2.49) μg/dl) compared to barely detectable plasma T4 levels in non-transplanted animals

250 (0.11 (0.06-0.23) μg/dl), however still lower than controls non-irradiated (3.63 (3.35-3.80)
251 (Fig. 4c). Evidence of functionality of the transplanted tissue is also provided by
252 immunostaining for T4, which shows numerous active follicles with strong T4 signal in the
253 luminal compartment (Fig. 4d). Considering the challenges of inducing thyroid ablation and
254 transplanting human cells in immunodeficient mice, which are highly sensitive to radiations
255 [38,39], here we present a proof of concept trial showing that human functional thyroid tissue
256 generated from pluripotent stem cells can be grafted and keep the functionality *in vivo*,
257 producing THs and increasing T4 levels in hypothyroid animals.
258

259 **Conclusions and perspectives**

260 The generation of functional human thyroid follicles *in vitro* has proven to be extremely
261 challenging, compared to mouse-derived equivalents. Although the generation of thyrocytes or
262 thyroid follicles from human stem cells has been reported [10–14], the present study is the first to
263 demonstrate hESC-derived thyroid follicles that produce TH *in vitro* and *in vivo* after
264 transplantation into thyroid gland ablated mice. Our model of human thyroid organoids that
265 function upon transplantation provides valuable source of knowledge to improve our
266 understanding of gene expression dynamics and mechanisms involved in thyroid
267 differentiation and maturation. It could be used as a new diagnostic tool to study of the
268 mechanisms leading to congenital hypothyroidism. Moreover, this model, although still in need
269 of improvement, provides a proof of concept that generating autologous human thyroid tissue
270 to maintain TH is within reach.
271

272 **METHODS SUMMARY**

273

274 The human NKX2-1$^{WT/GFP}$ ESC line [25] was genetically engineered to integrate the sequences
275 of *NXK2-1* and *PAX8* genes using lentivirus infection produced with the TRE/rtTA_NKX2-1-
276 PAX8 vector (Extended data Fig. 1b). The modified hESC were cultured in embryoid bodies
277 (EBs) using the hanging drop method [20], embedded in growth factor-reduced Matrigel, and
278 cultured in 12-well plates. Subsequent exposure to Activin A (AA), Doxycycline (Dox),
279 cAMP, rhTSH, dexamethasone, and SB431542 was performed as described in Fig. 1a. During
280 *in vitro* differentiation, organoids were subjected to extensive transcriptomic characterization
281 by qRT-PCR, bulk RNAseq, and single-cell RNAseq, while morphological changes were
282 assessed by live imaging and immunofluorescence. NKX2-1^{GFP+} cell population expansion and
283 proliferation were quantitatively measured by flow cytometry. *In vivo* studies were performed
284 using NOD-SCID mice, who's thyroid glands were ablated as previously described [16,41]. For
285 the transplantation studies, cultures were digested with a collagenase/dispase enzyme solution
286 for 45 days and the enriched ESC-derived thyroid follicular population was transplanted under
287 the kidney capsule. SPECT-CT images were acquired 4 weeks after transplantation, while T4
288 plasma levels and histological analyzes were performed 5 weeks after transplantation.
289

290 **References**

291 1. Vanderpump, M. P. J. The epidemiology of thyroid disease. *British Medical Bulletin* **99**,
292 39–51 (2011).
293 2. Garmendia Madariaga, A., Santos Palacios, S., Guillén-Grima, F. & Galofré, J. C. The
294 Incidence and Prevalence of Thyroid Dysfunction in Europe: A Meta-Analysis. *The*
295 *Journal of Clinical Endocrinology & Metabolism* **99**, 923–931 (2014).
296 3. Taylor, P. N. *et al.* Global epidemiology of hyperthyroidism and hypothyroidism.
297 *Nature Reviews Endocrinology* vol. 14 301–316 (2018).

298 4. Dew, R. *et al.* Clinical, behavioural and pharmacogenomic factors influencing the
299 response to levothyroxine therapy in patients with primary hypothyroidism-protocol for
300 a systematic review. *Systematic reviews* **6**, 60 (2017).
301 5. Kraut, E. & Farahani, P. A Systematic Review of Clinical Practice Guidelines'
302 Recommendations on Levothyroxine Therapy Alone versus Combination Therapy (LT4
303 plus LT3) for Hypothyroidism. *Clinical & Investigative Medicine* **38**, (2015).
304 6. Watt, T. *et al.* The thyroid-related quality of life measure ThyPRO has good
305 responsiveness and ability to detect relevant treatment effects. *Journal of Clinical*
306 *Endocrinology and Metabolism* **99**, 3708–3717 (2014).
307 7. Saravanan, P. *et al. Psychological well-being in patients on "adequate" doses of L-*
308 *thyroxine: results of a large, controlled community-based questionnaire study*. *Clinical*
309 *Endocrinology* vol. 57 (2002).
310 8. Clevers, H. Modeling Development and Disease with Organoids. *Cell* vol. 165 1586–
311 1597 (2016).
312 9. Kim, J., Koo, B. K. & Knoblich, J. A. Human organoids: model systems for human
313 biology and medicine. *Nature Reviews Molecular Cell Biology* vol. 21 571–584 (2020).
314 10. Kurmann, A. A. *et al.* Regeneration of Thyroid Function by Transplantation of
315 Differentiated Pluripotent Stem Cells. *Cell Stem Cell* **17**, 527–542 (2015).
316 11. Ma, R., Latif, R. & Davies, T. F. Human embryonic stem cells form functional thyroid
317 follicles. *Thyroid : official journal of the American Thyroid Association* **25**, 455–461
318 (2015).
319 12. Ma, R., Morshed, S. A., Latif, R. & Davies, T. F. TAZ Induction Directs Differentiation
320 of Thyroid Follicular Cells from Human Embryonic Stem Cells. *Thyroid : official*
321 *journal of the American Thyroid Association* **27**, 292–299 (2017).

322 13. Serra, M. *et al.* Pluripotent stem cell differentiation reveals distinct developmental
323 pathways regulating Lung-Versus Thyroid-Lineage specification. *Development*
324 *(Cambridge)* **144**, 3879–3893 (2017).
325 14. Ma, R., Shi, R., Morshed, S. A., Latif, R. & Davies, T. F. Derivation and 97%
326 Purification of Human Thyroid Cells From Dermal Fibroblasts. *Frontiers in*
327 *endocrinology* **11**, 446 (2020).
328 15. Ogundipe, V. M. L. *et al.* Generation and Differentiation of Adult Tissue-Derived
329 Human Thyroid Organoids. *Stem Cell Reports* **16**, 913–925 (2021).
330 16. Antonica, F. *et al.* Generation of functional thyroid from embryonic stem cells. *Nature*
331 **491**, 66–71 (2012).
332 17. Longmire, T. A. *et al.* Efficient derivation of purified lung and thyroid progenitors from
333 embryonic stem cells. *Cell Stem Cell* **10**, 398–411 (2012).
334 18. Ma, R., Latif, R. & Davies, T. F. Thyroid follicle formation and thyroglobulin expression
335 in multipotent endodermal stem cells. *Thyroid* **23**, 385–391 (2013).
336 19. Dame, K. *et al.* Thyroid Progenitors Are Robustly Derived from Embryonic Stem Cells
337 through Transient, Developmental Stage-Specific Overexpression of Nkx2-1. *Stem Cell*
338 *Reports* **8**, 216–225 (2017).
339 20. Bondue, A. *et al.* Mesp1 Acts as a Master Regulator of Multipotent Cardiovascular
340 Progenitor Specification. *Cell Stem Cell* **3**, 69–84 (2008).
341 21. Mazzoni, E. O. *et al.* Synergistic binding of transcription factors to cell-specific
342 enhancers programs motor neuron identity. *Nature neuroscience* **16**, 1219–1227 (2013).
343 22. Moreau, T. *et al.* Large-scale production of megakaryocytes from human pluripotent
344 stem cells by chemically defined forward programming. *Nature communications* **7**,
345 11208 (2016).

346 23. Pawlowski, M. *et al.* Inducible and Deterministic Forward Programming of Human
347 Pluripotent Stem Cells into Neurons, Skeletal Myocytes, and Oligodendrocytes. *Stem*
348 *cell reports* **8**, 803–812 (2017).
349 24. de Felice, M. & di Lauro, R. Thyroid development and its disorders: Genetics and
350 molecular mechanisms. *Endocrine Reviews* vol. 25 722–746 (2004).
351 25. Goulburn, A. L. *et al.* A targeted NKX2.1 human embryonic stem cell reporter line
352 enables identification of human basal forebrain derivatives. *Stem Cells* **29**, 462–473
353 (2011).
354 26. Vassart, G. & Dumont, J. E. *The Thyrotropin Receptor and the Regulation of Thyrocyte*
355 *Function and Growth**. vol. 13 (1992).
356 27. Mori, K., Mori, M., Stone, S., Braverman, L. & DeVito, W. Increased expression of
357 tumor necrosis factor-alpha and decreased expression of thyroglobulin and thyroid
358 peroxidase mRNA levels in the thyroids of iodide-treated BB/Wor rats. *European*
359 *Journal of Endocrinology* **139**, (1998).
360 28. Dohán, O. *et al.* The sodium/iodide symporter (NIS): Characterization, regulation, and
361 medical significance. *Endocrine Reviews* vol. 24 48–77 (2003).
362 29. Mincione, G. *et al.* EGF and TGF-β1 effects on thyroid function. *Journal of Thyroid*
363 *Research* vol. 2011 (2011).
364 30. Faria, M. *et al.* TNFα-mediated activation of NF-κB downregulates sodium-iodide
365 symporter expression in thyroid cells. *PloS one* **15**, e0228794–e0228794 (2020).
366 31. Romitti, M. *et al.* Single-Cell Trajectory Inference Guided Enhancement of Thyroid
367 Maturation In Vitro Using TGF-Beta Inhibition. *Frontiers in Endocrinology* **12**, (2021).
368 32. Fernández, L. P., López-Márquez, A. & Santisteban, P. Thyroid transcription factors in
369 development, differentiation and disease. *Nature Reviews Endocrinology* vol. 11 29–42
370 (2015).

371 33. Dom, G. *et al.* Transcriptomic Signature of Human Embryonic Thyroid Reveals
372 Transition From Differentiation to Functional Maturation. *Frontiers in Cell and*
373 *Developmental Biology* **9**, (2021).
374 34. Lazzaro, D., Price, M., de Felice, M. & Lauro, R. di. *The transcription factor TTF-1 is*
375 *expressed at the onset of thyroid and lung morphogenesis and in restricted regions of*
376 *the foetal brain*. *Development* vol. 113 (1991).
377 35. Haerlingen, B. *et al.* Small-Molecule Screening in Zebrafish Embryos Identifies
378 Signaling Pathways Regulating Early Thyroid Development. *Thyroid* **29**, (2019).
379 36. Vandernoot, I. *et al.* Enhanced Canonical Wnt Signaling During Early Zebrafish
380 Development Perturbs the Interaction of Cardiac Mesoderm and Pharyngeal Endoderm
381 and Causes Thyroid Specification Defects. *Thyroid* **31**, (2021).
382 37. Smith, T. J. Insulin-Like Growth Factor Pathway and the Thyroid. *Frontiers in*
383 *endocrinology* **12**, 653627 (2021).
384 38. Fulop, G. M. & Phillips, R. A. The scid mutation in mice causes a general defect in DNA
385 repair. *Nature* **347**, (1990).
386 39. Biedermann, K. A., Sun, J. R., Giaccia, A. J., Tosto, L. M. & Brown, J. M. scid mutation
387 in mice confers hypersensitivity to ionizing radiation and a deficiency in DNA double-
388 strand break repair. *Proceedings of the National Academy of Sciences of the United*
389 *States of America* **88**, 1394–1397 (1991).
390 40. Brandt, M. P. *et al.* Micro-single-photon emission computed tomography image
391 acquisition and quantification of sodium-iodide symporter-mediated radionuclide
392 accumulation in mouse thyroid and salivary glands. *Thyroid* **22**, 617–624 (2012).
393 41. Abel, E. D. *et al.* Divergent roles for thyroid hormone receptor β isoforms in the
394 endocrine axis and auditory system. *Journal of Clinical Investigation* **104**, (1999).
395

396 **Figures**

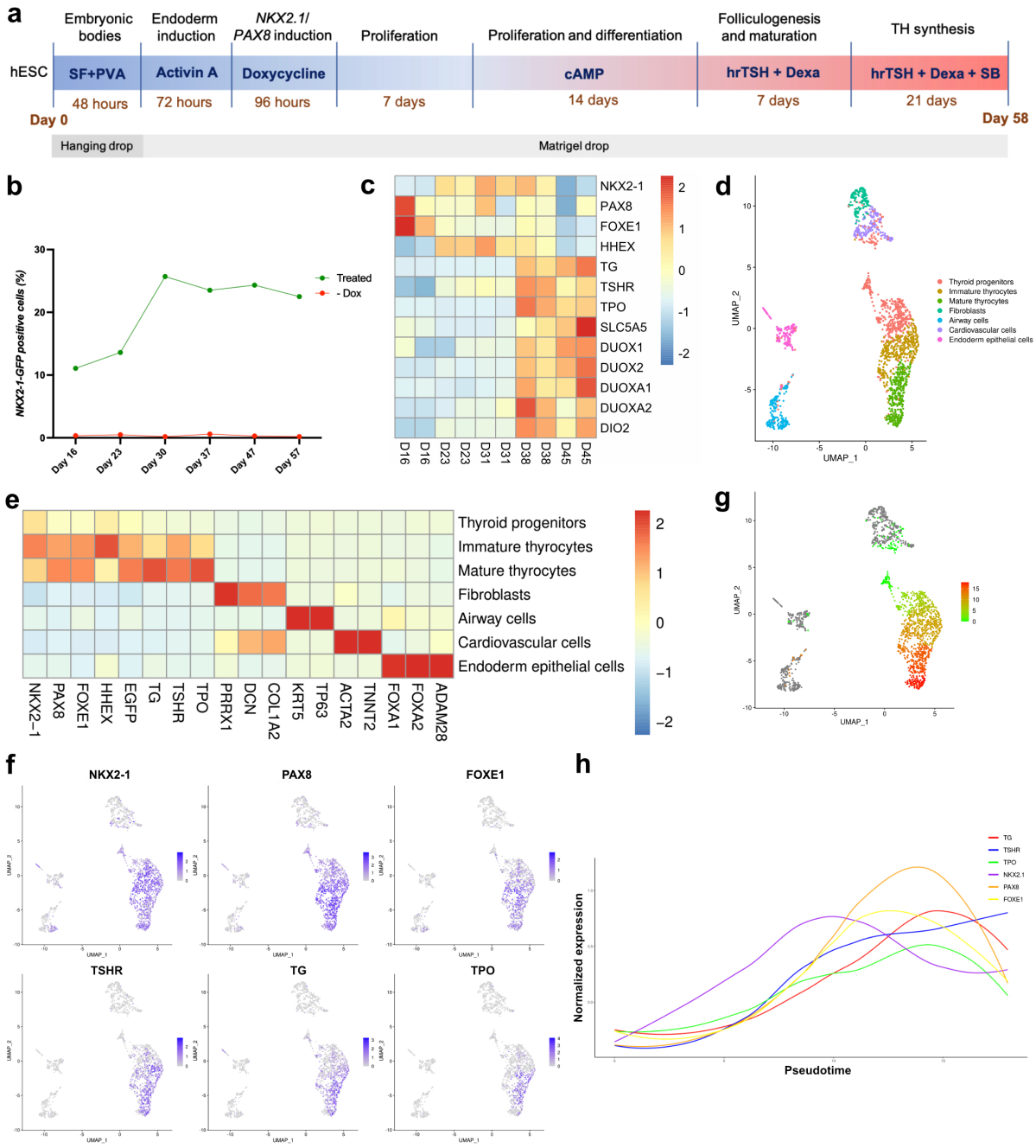

397

398 **Figure 1. Transient overexpression of *NKX2-1* and *PAX8* promotes differentiation of**
399 **human ESCs into thyroid follicular cells.** (a) Schematic representation of the protocol
400 leading to thyroid follicle differentiation from human ESCs. (b) Quantification by flow
401 cytometry of the proportion of NKX2-1^{GFP+} cells during the differentiation protocol. (c)
402 Heatmap of normalized bulk RNA-Seq expression of thyroid genes in NKX2-1^{GFP+} cells at

403 different stages of the thyroid differentiation protocol. Rows represent markers and columns
404 represent specific time points. Color values in the heatmap represent mean expression levels.
405 (d) Single cell RNA-Seq unsupervised clustering of *in vitro* derived human thyroid organoid
406 model cells (day 45). Each cluster is represented by a specific color. (e) Heatmap showing
407 normalized expression of selected marker genes with rows representing cell clusters, while
408 columns represent genes. The intensity of the color in each square indicates the mean
409 expression within the cluster. (f) UMAP overlaid with gene expression plots for thyrocyte
410 markers. Color indicates normalized expression. (g) Diffusion analysis of thyrocyte lineage
411 with thyroid progenitor cells as root cells. UMAP overlaid with pseudotime. Color in
412 pseudotime plot indicates order of cell progression. (h) Expression trends of thyroid genes
413 along the pseudotime trajectory.
414
415
416
417
418

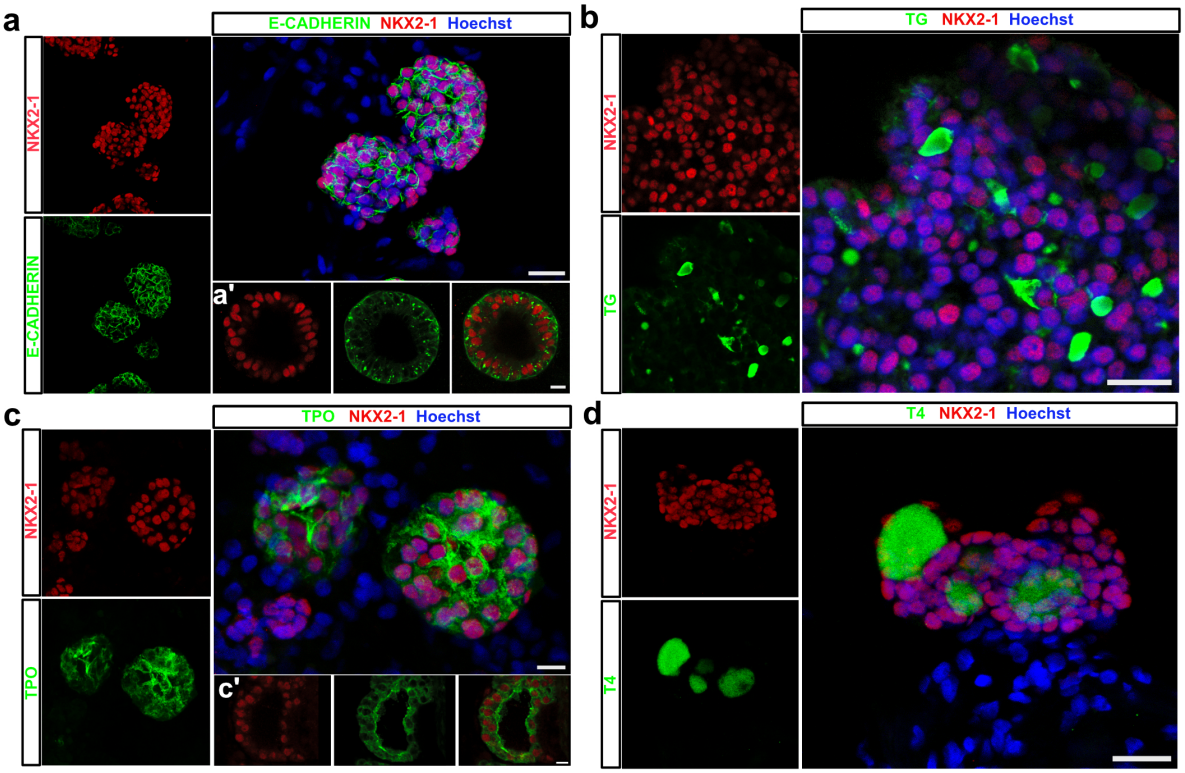

Figure 2. Characterization of human ESC-derived thyroid follicular structures by immunostaining. (a-d) Confocal immunofluorescence images at day 58 of the differentiation protocol. Three-dimensional follicular structures co-expressing NKX2-1 and (a) E-CADHERIN (a'; follicle at high magnification), (b) TG with cytosolic and luminal accumulation, (c) TPO cytoplasmic and apical membrane expression (c'; follicle at high magnification), and (d) T4 storage in the lumenal compartment. Scale bars, 20 µm and 10 µm for high magnification follicles.

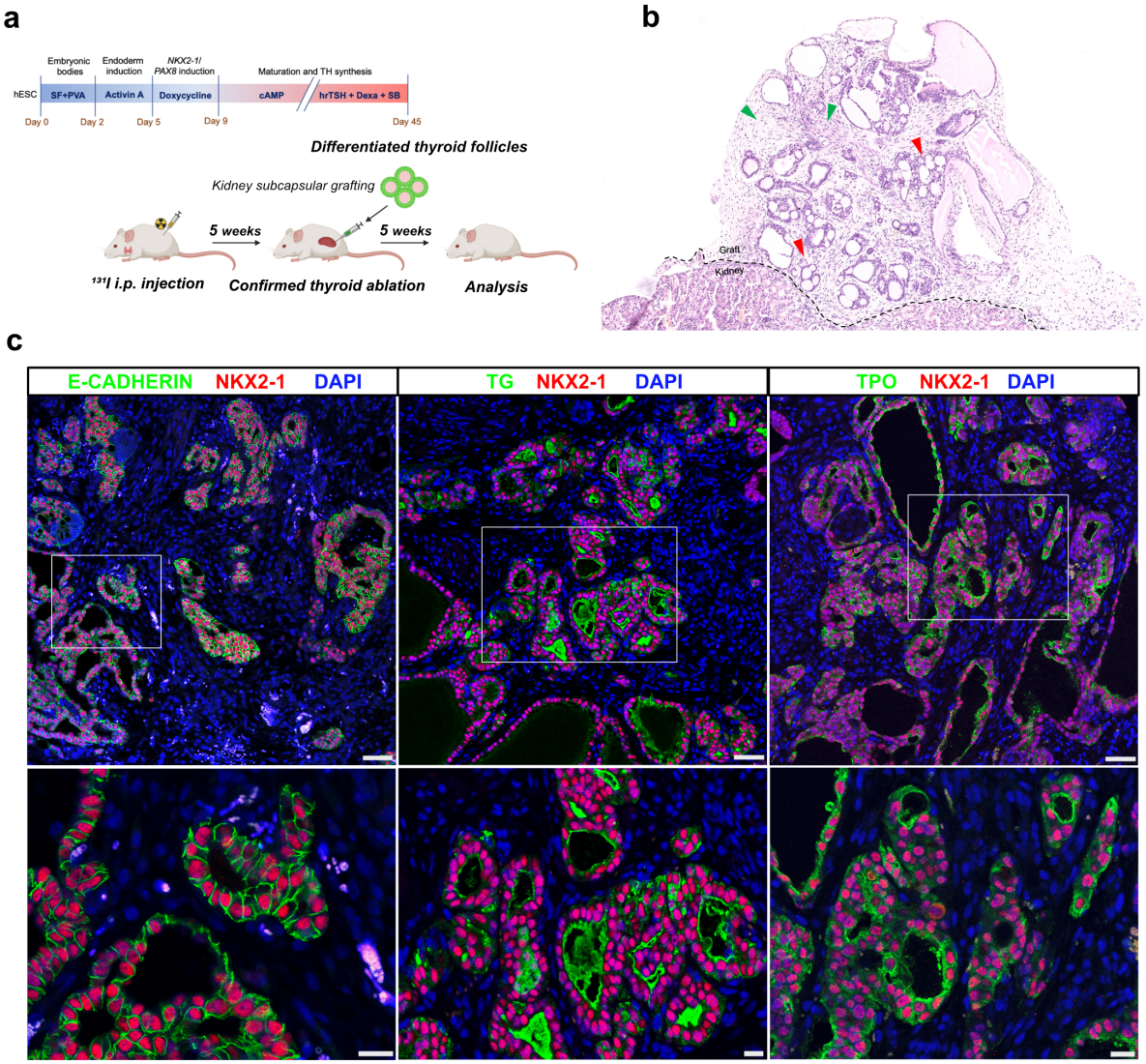

427

428 **Figure 3. Transplantation of hESC-derived enriched thyroid follicles into NOD-SCID**
429 **mice.** (a) Schematic representation of the hESC-derived thyroid follicles transplantation \under
430 the kidney capsule protocol in NOD-SCID untreated mice or previously thyroid RAI ablated
431 by intraperitoneal ^{131}I injection. (b-c) Histological analysis of the grafted sections 5 weeks after
432 transplantation. (b) Hematoxylin and eosin-stained sections of the transplanted organoids show
433 the localization of the generated human thyroid follicles in the cortical region of the host
434 kidney. Red arrows show the organization of the monolayer epithelium of the transplanted
435 tissue surrounded by stromal cells (green arrows). (c) Confocal images show co-expression of
436 NKX2-1 and E-CADHERIN in the monolayered epithelially organized follicular structures.

437 The grafted tissue shows that TG is principally accumulated in the luminal compartment,
438 whereas TPO is strongly expressed in the apical membrane. Scale bars, 50μm (upper images)
439 and 20μm (zoomed lower images).
440

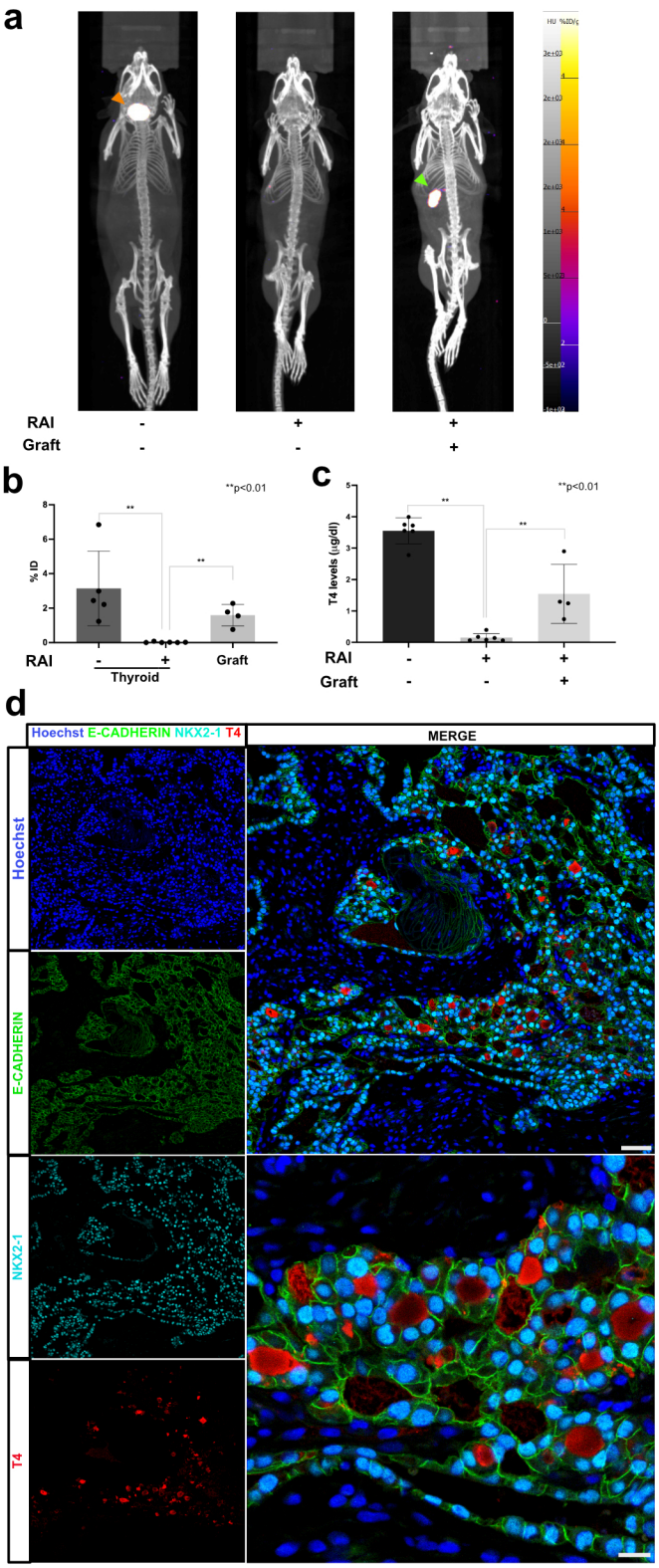

Figure 4. *In vivo* functionality of transplanted human ESC-derived thyroid follicles. (a) Maximum intensity projections generated from SPEC/CT images of non-irradiated and non-transplanted (left), RAI-ablated and non-transplanted (middle), and RAI-ablated and

445 transplanted (right) mice. Images were obtained four weeks after organoids transplantation.
446 The ^{123}I uptake in the mouse thyroid tissue is shown by the orange arrow, while the signal from
447 the human thyroid tissue (graft) is highlighted by the green arrow. The color scales are chosen
448 to represent the radioactivity uptake in PET images expressed as standardized uptake values
449 (SUV) (0 to 8, from light yellow to dark blue). (b) Quantification of ^{123}I uptake in SPECT
450 images expressed as percentage of injected dose (% ID) in the intact (non-irradiated) (2.44
451 (1.72-4.91) % ID; n=5) or RAI-ablated thyroid region (0.01 (0.002-0.03) % ID; n=6), and
452 grafted tissue (1.66 (0.96-2.14) % ID; n=4). (c) Comparison of plasma T4 levels among
453 controls (3.63 (3.35-3.80) μg/dl; n=6), irradiated/non-transplanted (0.11 (0.06-0.23) μg/dl;
454 n=6) and irradiated/transplanted mice (1.26 (0.86-2.49) μg/dl; n=4). (d) NKX2-1, E-
455 CADHERIN and T4 immunostaining demonstrate the presence of hESC-derived follicles in
456 the transplanted area with specific accumulation of T4 within the lumen of several structures.
457 Mann-Whitney test was used for statistical analysis. **$p<0.01$.
458
459
460
461
462
463
464
465
466
467
468
469

470 **Extended data**

471

472 **METHODS**

473

474 **Generation of tetracycline-induced hESC line:** The human embryonic stem cell line HES3
475 used in this study was genetically modified at the NKX2-1 locus to allow insertion of sequences
476 encoding green fluorescent protein (GFP), resulting in the NKX2-1$^{wt/GFP}$ hESC line as
477 previously described [25] (Extended data Fig. 1a). To generate an inducible NKX2-1-PAX8
478 hESC line, we cloned the coding sequences of the *NKX2-1* and *PAX8* genes, separated by a
479 IRES sequence, into the pInducer20 lentiviral vector (a gift from Stephen Elledge; Addgene
480 plasmid # 44012; http://n2t.net/addgene:44012; RRID: Addgene_44012), which contains the
481 sequences for the TRE/rtTA-inducible system (Extended data Fig. 1b). Lentiviral supernatants
482 were generated by transient transfection of HEK293 cells according to Lipofectamine ™ 2000
483 (Invitrogen) transfection protocols and harvested 48 h after transfection. To promote
484 integration of sequences into the genome of the NKX2-1$^{wt/GFP}$ HES3 line, hESCs were plated
485 at high density (1:3) in a Matrigel-coated 6-well culture dish and infected with 50 ml of
486 lentivirus supernatant and 6 μg/ml polybrene for 18-20 hours in mTeSR medium (Stem Cell).
487 Positive clones were selected with 300 μg/ml neomycin (Invitrogen). Clones were treated with
488 1 mg/ml doxycycline (Sigma) for 48 h and screened by immunostaining against NKX2-1 and
489 PAX8 to verify transgene expression. Selected clones were tested for genomic integrity using
490 G-banding technique according to the protocol described previously [42]. Pluripotency was
491 assessed by testing the ability of the clones to differentiate into cells from the three germ layers.
492 Cells were cultured in basal differentiation medium (Extended data Table 1) for 21 days and
493 the formation of endoderm, mesoderm and ectoderm cells was assessed by
494 immunofluorescence staining against AFP, α-SMA and β-III tubulin, respectively. The hESC-

495 NKX2-1-PAX8 line was registered and approved by the European Human Pluripotent Stem
496 Cell Registry (hPSCreg) as ESIBIe003-A-6.
497
498 **hESC culture and differentiation:** Modified hESCs were cultured and propagated on
499 Matrigel-coated 6-well culture dishes in Stem Flex medium (Thermo Scientific, A3349401)
500 supplemented with 100 U/ml Penicillin-Streptomycin (Gibco). For the generation of embryoid
501 bodies (EBs), highly confluent hESCs were detached with 0.5 mM EDTA solution and diluted
502 with 100,000 cells/ml in Stem Flex medium supplemented with 4 mg/ml polyvinyl alcohol
503 (PVA; Sigma) and EBs formation was induced as previously described [16,20]. Briefly, hESCs
504 (2,000 cells per droplet) were cultured in hanging drops for two days, then EBs were collected
505 and embedded in growth factor-reduced Matrigel (BD Biosciences); 50 µl Matrigel drops
506 (containing approximately 20 embryoid bodies per drop) were replated onto 12-well dishes.
507 Embryoid bodies were differentiated and cultured in differentiation medium containing
508 DMEM/F12+Glutamax (Gibco) with 20% FBS (Gibco), 0.1 mM non-essential amino acids
509 (Gibco), 1 mM sodium pyruvate (Gibco), 0.1 mM 2-mercaptoethanol (Sigma), 100 U/ml
510 Penicillin-Streptomycin (Gibco), and 50 µg/ml L-ascorbic acid (Sigma). Cells were
511 supplemented with 50 ng/ml Activin A (Cell GS) for three days to induce foregut endoderm.
512 Expression of *NKX2-1* and *PAX8* was induced by incubation with 1 mg/ml doxycycline (Dox;
513 Sigma) for four days. Cells were then cultured in basal differentiation medium for one week to
514 allow expansion of thyroid progenitors, while differentiation and maturation were induced by
515 treatment with 300 µM 8-br-cAMP (Biolog Inc.), 1 mU/ml rhTSH (Genzyme), 50 nM
516 dexamethasone (Dexa; Sigma) and 10 µM SB431542 (Peprotech) where indicated (Figure 1a).
517 Culture medium was changed every 48 hours.
518

519 **NKX2-1^{GFP+} population assessment – Flow cytometry:** hESCs under the thyroid
520 differentiation protocol were collected each week, from day 16 to day 45, and prepared for
521 flow cytometry immunostaining as follows: Matrigel drops (at least 4 samples per time point)
522 were first digested with HBSS solution containing 10 U/ml dispase II (Roche) and 125 U/ml
523 collagenase type IV (Gibco, Thermo Fisher) for 30-60 min at 37°C; then a single cell
524 suspension was obtained by dissociation with TripLE Express (Thermo Fisher) for 10-15 min
525 incubation at 37°C, the enzymes were inactivated by addition of differentiation medium. After
526 centrifugation, samples were rinsed with PBS and fixed in 1.6% PFA solution in PBS for 15
527 min at RT, followed by cell permeabilization with 0.1% Triton solution in PBS for 15 min at
528 4°C under agitation. After centrifugation, 4% horse serum and 0.5% Tween 20 PBS blocking
529 solution was added for 10 min (4°C with shaking). The primary anti-rabbit KI67 antibody
530 (1:100) was diluted in the blocking solution and samples were incubated for 30 min (4°C with
531 shaking). Cells were then rinsed three times with wash solution (0.5% BSA and 0.5% Tween
532 in PBS) and then incubated with Cy5-conjugated anti-rabbit antibody (1:300) diluted in
533 blocking solution for 30 min (4°C with shaking). NKX2-1^{GFP+} and K67 expression data were
534 obtained and processed using an LSR-Fortessa X-20 flow cytometer and FACSDiva software
535 (BD Biosciences). Unstained cells and isotype controls were included in all experiments. In
536 addition, the percentage of GFP+ cells was used to estimate the thyroid generation efficiency
537 of our protocol.
538
539 **RNA extraction and quantitative real-time PCR:** For total RNA extraction, human
540 organoids (at different time points), *in vivo* samples, and human thyroid tissue (histologicaly
541 normal thyroid tissue was obtained from a patient undergoing thyroidectomy; Hopital Erasme-
542 ULB Ethics Committee approval; P2016/260), was lysed using RLT lysis buffer supplemented
543 with 1% 2-mercaptoethanol (Sigma), and RNA isolation was performed using the RNeasy

544 micro kit (Qiagen) according to the manufacturer's instructions. For reverse transcription, the
545 Superscript II kit (Invitrogen) was used, and qPCR was performed in triplicates using Takyon
546 (Eurogentec) and CFX Connect Real-Time System (Biorad). Results are presented as
547 linearized values normalized to housekeeping gene, GAPDH (human) or β2-microglobulin
548 (mouse) and the indicated reference value (2-ΔΔCt). Gene expression profile was obtained
549 from at least three independent experiments. Primer sequences are shown in Table 3.
550
551 **RNA-seq and analysis of bulk samples:** Bulk RNA-seq was performed in hESC-
552 differentiated cells every week from day 16 to day 45 of our differentiation protocol (Figure
553 1a). The NKX2-1^{GFP+} cell population was obtained by FACS sorting (FACS Aria; BD
554 Bioscience) after sample preparation was performed as previously described (section "NKX2-
555 1^{GFP+} population expansion assessment - Flow Cytometry"). In brief, 10,000 NKX2-1^{GFP+} cells
556 were directly sorted into 700 µl of Qiazol lysis reagent (Qiagen) and RNA isolation was
557 performed using the miRNeasy micro kit (Qiagen) according to the manufacturer's instructions.
558 RNA concentration and quality were evaluated using Bioanalyser 2100 (Agilent) and RNA
559 6000 Nano Kit (Agilent). RNA integrity was preserved, and no genomic DNA contamination
560 was detected. Ovarion Solo RNA-seq Systems (NuGen) was used as indicated by the
561 manufacturer, resulting in high-quality indexed cDNA libraries quantified with the Quant-iT
562 PicoGreen kit (Life Sciences) and Infinite F200 Pro plate reader (Tecan); DNA fragment size
563 distribution was examined with the 2100 Bioanalyzer (Agilent) using the DNA 1000 kit
564 (Agilent). Multiplexed libraries (10ρM) were loaded onto flow cells and sequenced on the
565 HiSeq 1500 system (Illumina) in high-output mode using the HiSeq Cluster Kit v4 (Illumina).
566 Approximately 10 million paired-end reads were obtained per sample. After removal of low-
567 quality bases and Illumina adapter sequences using Trimmomatic software [43], sequence reads
568 were aligned against the human reference genome (Hg19) using HiSat2 software [44]. Raw reads

569 were determined with HTSeq software [45] using the Ensembl genome annotation GRCh38.p13.
570 Normalization and differential expression analyzes were performed with two biological
571 replicates per sample using the website iDEP version 0.93 [46]. Genes for which expression
572 values were lower than 5 were filtered out. The fold changes of mean gene expression for the
573 duplicates were used to calculate the level of differential gene expression.
574
575 **Single cell RNAseq characterization of thyroid organoids:** Cells originating from human
576 thyroid differentiation protocol, at day 45, were isolated for scRNAseq profiling, following the
577 procedures previously described [31]. Single cell suspension preparation and FACS cell sorting
578 were performed as previously mentioned ("Cell proliferation assessment – Flow cytometry"
579 and RNA-seq and analysis of bulk samples sections). Different proportions of viable NKX2-
580 1/GFP+ (60%) and NKX2-1/GFP- (40%) cells were sorted to guarantee representation of the
581 distinct cell types present in the organoid culture. Sorted cells were collected in PBS at a density
582 of 800cells/ul and diluted accordingly to kit's instruction (10x Genomics Chromium Single
583 Cell 3' v3). Around 6,000 cells were loaded onto a channel of the Chromium Single Cell 3′
584 microfluidic chip and barcoded with a 10X Chromium controller followed by RNA reverse
585 transcription and amplification according to manufacturer's recommendations (10X
586 Genomics). Library preparation was performed based on 10x Genomics guidelines. Libraries
587 were sequenced using Illumina NovaSeq 6000 system.
588
589 **Single cell RNAseq data analysis:** Raw sequencing data was aligned, annotated,
590 demultiplexed and filtered using Cell Ranger Software (v.6.0.1) with a custom-built reference.
591 The custom-built reference was based on the human reference genome GRCh38 and gene
592 annotation Ensembl 98 in which the EGFP sequence was included. The new reference was
593 generated using the cellranger mkref function from the Cell Ranger Software. Analyses were

done using R 4.1.0 and Seurat version 4.0.3 [47]. Briefly, raw counts from Cell Ranger were loaded and the "background soup" was removed using SoupX [48]. The background soup refers to ambient RNA molecules contaminating cell-containing droplets, a common problem in droplet-based single cell RNA-sequencing technologies. Decontaminated UMIs were then filtered to discard any doublet (droplet containing two cells instead of 1) using DoubletFinder [49]. Finally, cells containing less than 200 unique genes or more than 26% of UMI counts related to mitochondrial genes were discarded. The 26% threshold was selected to discard dying cells while retaining as much barcodes as possible. The resulting library was scaled and normalized using the SCTransform function from Seurat. Cell cycle effects and mitochondrial content were used as variables to regress out with SCTransform. Principal component analysis (PCA) was computed using the 3000 first variable features, and the top 30 principal components were used for SNN graph construction, clustering (resolution 1) and UMAP embedding using Seurat's functions and recommended methods. Cluster annotation was based on marker genes obtained using Seurat's FindAllMarkers function and literature survey. Pseudotime analysis in thyroid populations was performed using Monocle3 [50] with default parameters and with data imported from the Seurat object, selecting thyroid progenitors as root cells. Pseudotime-related plots were generated using the FeaturePlot function from Seurat and the geom_smooth function from ggplot2. Receptor-ligand interaction analysis was done with CellPhoneDB, which consists in a public repository of ligands, receptors and their interactions enabling a comprehensive and systematic analysis of cell–cell communication [51]. CellphoneDB was run using the statistical method with default parameters. A manually selected list of biologically relevant ligand-receptor pairs displaying statistically significant interaction was used to create the dot plot showing the interactions of thyroid populations with other cell populations.

618 **Follicles enrichment for *in vivo* transplantation:** Thyroid organoids at day 45 of
619 differentiation were washed twice with Hanks's balanced salt solution (HBSS, containing
620 calcium and magnesium; Gibco), then 1 ml of a digestion medium containing 10 U ml dispase
621 II (Roche) and 125 U ml of collagenase type IV (Sigma) diluted in HBSS was added to each
622 well. The organoids were carefully removed using a 5 ml pipette and transferred to a sterile
623 Erlenmeyer and incubated at 37 °C in a water bath with shaking for 45 - 60 min. The release
624 of thyroid follicles was tracked by microscopy (bright field and GFP). When isolated structures
625 were detected, enzymes were inactivated by addition of 10% FBS followed by centrifugation
626 at 500 g for 3 min. Cells were rinsed twice with HBSS and the follicles population was enriched
627 using 30 µm (single cell removal) and 100 µm (follicles enrichment; 30-100 µm size) reverse
628 strainer (Pluriselect). Finally, the 3D-structures were counted and approximately 10,000
629 structures were resuspended in 65 µl of differentiation medium for *in vivo* transplantation.
630
631 **RAI-induced hypothyroidism mouse generation, transplantation of hESC-derived**
632 **thyroid follicles and SPECT-CT imaging:** All animal experiments were performed in
633 accordance with local Animal Ethics (Ethical Project CMMI-2020-01). A cohort of 20 five-
634 week-old female non-obese and non-diabetic mice with severe combined immunodeficiency
635 (NOD -SCID) (Charles River Laboratories, France) was placed on an iodine-deficient diet for
636 one week after arrival. In addition, six NOD -SCID mice, not submitted to any treatment were
637 included in the study as external controls. One week after starting the diet (first week), 14 of
638 the 20 mice were injected intraperitoneally with approximately 5.75 MBq (90µL supplemented
639 with 10 µL NaCl 0.9% solution (MiniPlasco, BBraun) Iodide ^{131}I-Injection-IBS.2P (GE
640 Healthcare Belux, Belgium). To confirm the destruction of functional thyroid tissue by ^{131}I
641 injection, SPECT-CT images of Sodium Iodide ^{123}I uptake were obtained on a nanoSPECTPlus
642 (for the SPECT) and a nanoScanPETCT (for the CT) (Mediso, Hungary) equipped with a

643 Minerve rat cell implemented with a mouse insert. In the fourth week, the 20 mice were injected
644 intravenously with 8.75-9.33 MBq ^{123}I 24 hours before imaging. SPECT/CT imaging was
645 performed on two mice in parallel under isoflurane anesthesia (1.8% isoflurane, 2.0 l/min O2)
646 with the following parameters: collimator aperture APT105, 'fast' helicoidal acquisition mode
647 with a duration of 50 s/projection to acquire 1000 counts per projection, scan range of 105 mm,
648 reconstruction in standard mode, i.e. 35% smoothing, 3 iterations and 3 subsets to obtain a
649 voxel size of 750 μm^3. CT was performed with the following parameters: 480 projections,
650 minimum zoom, binning 1:4, 50 kV, 300 ms/proj, scan range of 115 mm. Acquisition data
651 were reconstructed with a Feldkamp-based algorithm generated to obtain a cubic voxel of
652 250 μm^3, using a cosine filter with a cut-off of 100%. Then, one week later (week five) 6
653 irradiated mice were transplanted with thyroid organoids. First, control and thyroid gland
654 ablated mice were treated with 0.01 mg/ml - 50 µl Temgesic (Schering Plow), anesthetized
655 under isoflurane anesthesia, and the eyes/cornea were protected with Vidisic gel (Bausch &
656 Lomb Inc.). Mice were injected with 8 µl of follicle-enriched suspension thyroid organoids
657 (described in "Enrichment of follicles for *in vivo* transplantation") into the unilateral kidney
658 under the capsule using a 30G needle syringe (Hamilton Bonaduz AG) (the kidney was exposed
659 through skin/muscle/peritoneum incision via a dorsolateral approach). The entire cohort of
660 mice was imaged 4 weeks after transplantation (week 9) as described above to assess the iodine
661 uptake capacity of the transplanted tissue. Due to the radiosensitivity of immunodeficient mice
662 [38,39], 30% of the irradiated animals died during the experimental period. At the end of the
663 experiment (week ten), 6 non-transplanted and 4 transplanted mice had survived and could be
664 analyzed. Mice were finally sacrificed, blood collection was performed for the T4 assay, while
665 the kidney and transplanted tissues were harvested for transcriptomic and histological analyzes.
666 Qualitative and quantitative analysis of the images was performed using VivoQuant v3.5
667 software (InVicro, USA). Radioiodine uptake in thyroid tissue and/or graft was evaluated

668 according to the design of volumes of interest (VOI) based on the corresponding radioactive
669 signal. The % injected dose (% ID) was calculated as previously described by Brandt, et al,
670 2012 [40] and results were expressed as % ID/organ [40].
671
672 **Plasma T4 measurement:** Total T4 levels were measured by Mouse/Rat T4 Total ELISA kit
673 (T4044T-100 Calbiotech) according to the manufacturer's instructions.
674
675 **Immunofluorescence staining:** For immunofluorescence staining, cells cultured in monolayer
676 or MTG -drop were fixed in 4% paraformaldehyde (PFA; Sigma) for 2 h at RT, washed three
677 times in PBS, and blocked in 3% bovine serum albumin (BSA; Sigma), 5% horse serum
678 (Invitrogen), and 0.3% Triton X-100 (Sigma) PBS solution for 30 min at room temperature.
679 Primary and secondary antibodies were diluted in a PBS solution of 3% BSA, 1% horse serum,
680 and 0.1% Triton X-100. Primary antibodies were incubated overnight at 4°C, then washed three
681 times and incubated with secondary antibodies for 2 h at room temperature. The nuclei were
682 stained with Hoechst 33342 (Invitrogen). The slides were mounted with Glycergel (Dako). For
683 paraffin embedding, *in vitro* organoids and grafted samples were fixed overnight at 4°C in 4%
684 PFA and kept in 70% ethanol at 4°C for at least 24 hours at 4°C before embedding. Samples
685 were then embedded in paraffin, sectioned (5 µm), mounted on glass slides, deparaffinized,
686 and rehydrated. For histological analysis, sections were stained with hematoxylin and eosin
687 (H&E) according to a routine protocol. For immunostaining, antigen retrieval was performed
688 by incubating the sections for 10 min in the microwave (850 W) in Sodium Citrate Buffer (10
689 mM Sodium Citrate, 0.05% Tween 20, pH 6.0). After cooling, the sections were rinsed with
690 PBS and then blocked with 1% BSA and 10% horse serum PBS solution for 1 h at RT. Primary
691 antibodies were diluted in the blocking solution and incubated overnight at 4°C. The sections
692 were rinsed three times in PBS and incubated with Hoechst 33342 (Invitrogen) and secondary

693 antibodies diluted in blocking solution for 1 h at room temperature. Slides were mounted with
694 Glycergel (Dako). Information on antibodies and sources are listed in Extended Data Table 2.
695
696 **Imaging:** Fluorescence imaging was performed on a Zeiss LSM510 META confocal
697 microscope, a Zeiss Axio Observer Z1 microscope with AxioCamMR3 camera, and a Leica
698 DMI6000 with DFC365FX camera. Hematoxylin and eosin whole slide images were acquired
699 using a NanoZoomer- SQ digital slide scanner C13140-01 (Hamamatsu) and images were
700 generated using NDP.view 2 software (Hamamatsu).
701
702 **Statistical analysis:** Statistical significance between two groups was tested using the unpaired
703 t test or the nonparametric Mann-Whitney U test, while comparison between multiple groups
704 was performed using one-way ANOVA or Kruskal-Wallis tests. Data are presented as mean ±
705 SD or median (IQR). Differences were considered significant at $p<0.05$. GraphPad Prism
706 version 9 was used for most analyses (GraphPad Software). Data presented are from at least
707 three independent experiments.
708
709 **Data availability**
710 Bulk RNA-seq and Single-cell RNA-seq data have been deposited in the NCBI Gene
711 Expression Omnibus under accession number GSE181452 and GSE181256, respectively.
712 Source data are provided with this paper.
713
714 **Code availability**
715 Custom computer script used to generate scRNAseq data are available upon request.
716
717

718 **Methods references**

719 42. Campos, P. B., Sartore, R. C., Abdalla, S. N. & Rehen, S. K. Chromosomal spread
720 preparation of human embryonic stem cells for karyotyping. *Journal of*
721 *Visualized Experiments* (2009) doi:10.3791/1512.

722 43. Bolger, A. M., Lohse, M. & Usadel, B. Trimmomatic: a flexible trimmer for
723 Illumina sequence data. *Bioinformatics* **30**, (2014).

724 44. Kim, D., Langmead, B. & Salzberg, S. L. HISAT: a fast spliced aligner with low
725 memory requirements. *Nature Methods* **12**, (2015).

726 45. Anders, S., Pyl, P. T. & Huber, W. HTSeq--a Python framework to work with
727 high-throughput sequencing data. *Bioinformatics* **31**, (2015).

728 46. Ge, S. X., Son, E. W. & Yao, R. iDEP: an integrated web application for
729 differential expression and pathway analysis of RNA-Seq data. *BMC*
730 *Bioinformatics* **19**, (2018).

731 47. Hao, Y. *et al.* Integrated analysis of multimodal single-cell data. *Cell* **184**, 3573-
732 3587.e29 (2021).

733 48. Young, M. D. & Behjati, S. SoupX removes ambient RNA contamination from
734 droplet-based single-cell RNA sequencing data. *GigaScience* **9**, (2020).

735 49. McGinnis, C. S., Murrow, L. M. & Gartner, Z. J. DoubletFinder: Doublet
736 Detection in Single-Cell RNA Sequencing Data Using Artificial Nearest
737 Neighbors. *Cell Systems* **8**, (2019).

738 50. Cao, J. *et al.* The single-cell transcriptional landscape of mammalian
739 organogenesis. *Nature* **566**, 496–502 (2019).

740 51. Efremova, M., Vento-Tormo, M., Teichmann, S. A. & Vento-Tormo, R.
741 CellPhoneDB: inferring cell–cell communication from combined expression of
742 multi-subunit ligand–receptor complexes. *Nature Protocols* **15**, (2020).

743 **Acknowledgements**

744 We acknowledge the ULB flow cytometry platform (Christine Dubois), the ULB genomic core
745 facility (F. Libert and A. Lefort), LiMIF platform for confocal microscopy (J.-M.
746 Vanderwinden), Coraline De Maeseneire, Nicolas Passon and Christophe Van Heymbeek
747 (CMMI) for their contribution for the *in vivo* studies. We also acknowledge Professor Andrew
748 G Elefanty for kindly providing human ESC cell line (HES3-NKX2-1$^{WT/GFP}$). Schematic
749 grafting diagram was created with BioRender.com.

750

751 **Author Contributions**

752 M.R. and S.C. developed the project, designed the experiments and analyzed the data. D.F.K
753 generated and selected the hESC-NKX2-1/Pax8 line. M.R., B.F.F and O.M. performed most
754 of the *in vitro* experiments and protocol set up. L.C. performed cell culture, maintenance and
755 karyotype analysis. S.C., M.R and G.D. executed *in vivo* studies. G.D., G.V.S. and S.G.
756 acquired SPECT-CT images and run the % ID analysis. M.R., B.F.F., H.L. analyzed RNA
757 expression and performed IF. P.G. obtained confocal images. M.R. and H.L. performed bulk
758 RNA-Sequencing and analyzed the results. M.R., S.P.S. and B.F.F performed the single-cell
759 RNA-Sequencing. A.T., V.D., B.F.F. S.P.S., S.E.E. and H.L. performed the bioinformatics
760 analysis. S.C. and M.R. wrote the first draft and S.P.S. and S.R. edited the manuscript. S.C.
761 and S.R. acquired funding for the project. All authors contributed to the article and approved
762 the submitted version.

763

764 **Competing interests:** The authors declare no competing interests.

765

766

767

Funding

This work was supported by grants from the Belgian National Fund for Scientific Research (FNRS) (PDR T.0140.14; PDR T.0230.18), the Fonds d'Encouragement à la Recherche de l'Université Libre de Bruxelles (FER-ULB) and it has received funding from the European Union's Horizon 2020 research and innovation programme under grant agreement No. 825745. M.R. was supported in part by the Brazilian National Council for Scientific and Technological Development (CNPq; Brazil). Work by S.P.S. was supported by MISU funding from the FNRS (34772792 – SCHISM). The Center for Microscopy and Molecular Imaging (CMMI) is supported by the European Regional Development Fund (ERDF), the Walloon Region, the Fondation ULB, the Fonds Erasme and "Association Vinçotte Nuclear" (AVN). G.D. is supported by European Regional Development Fund (ERDF) and the Walloon Region. M.R was supported by FNRS (Chargé de Recherche) and grant agreement No.825745. B.F.F. and S.R. were supported in part by grant DK15070 from The National Institutes of Health (USA). S.C is Research Director at FNRS.

Supplementary Information is available for this paper. Correspondence and requests for materials should be addressed to Sabine Costagliola: sabine.costagliola@ulb.be.

Extended Data

Figures

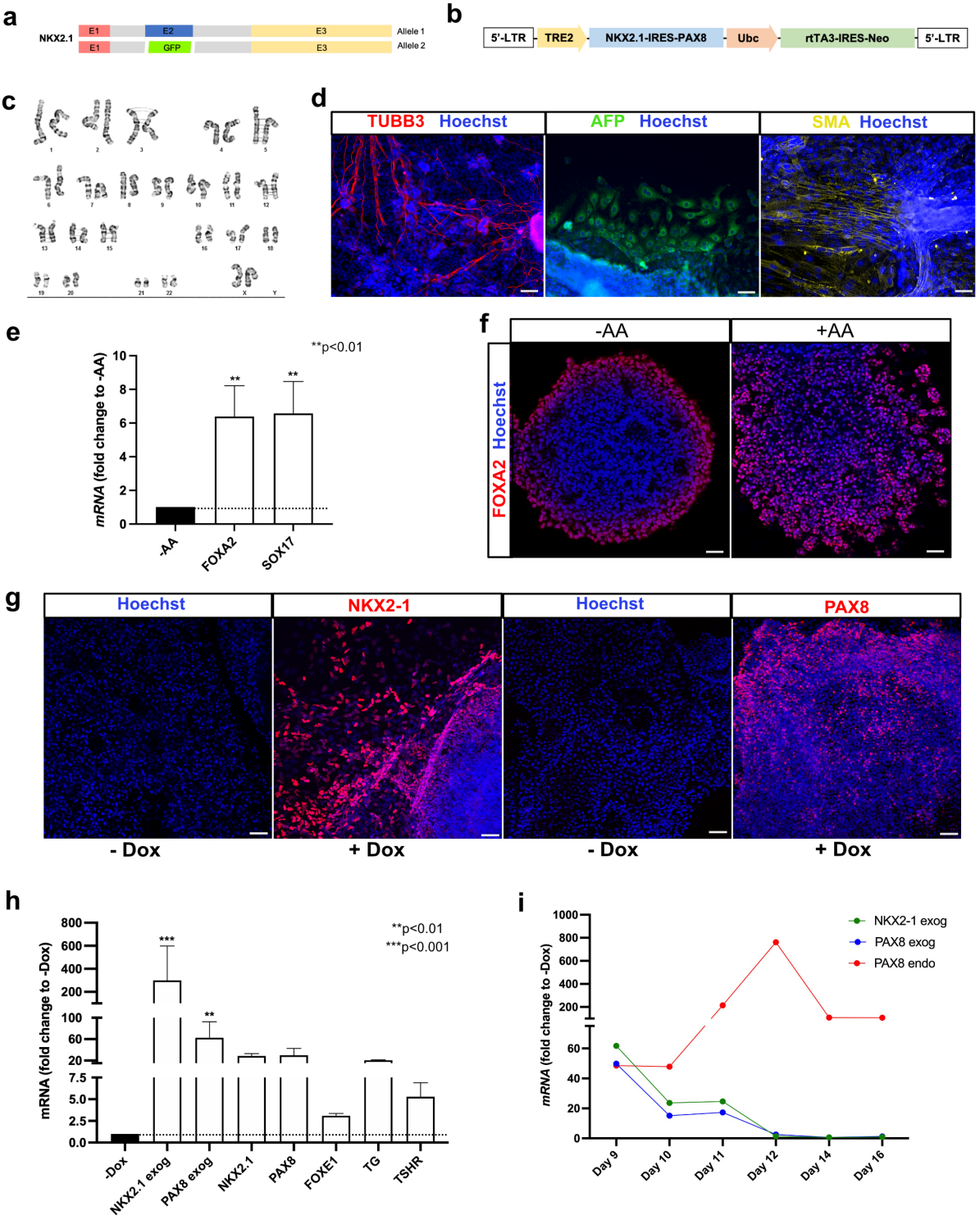

797 **Extended data Fig. 1. Generation, characterization and early differentiation of the**
798 **NKX21-PAX8 tetracycline-inducible human ESC line.** (a) Schematic representation of the
799 previously generated NKX2-1WT/GFP human ES cell line (Goulburn, 2011). (b) NKX21-
800 PAX8 tetracycline-inducible human ESC line was generated by cloning OFRs into the
801 pInducer20 lentivirus vector backbone. (c) Human ESCs showed normal karyotype after
802 genetic manipulations. (d) Modified hESCs showed maintenance of pluripotency by
803 spontaneous differentiation into ectoderm (TUBB3), endoderm (AFP) and mesoderm cells (a-
804 SMA). I *FOXA2* and *SOX17* mRNA levels after activin A (AA) treatment (day 5). (f)
805 Immunostaining shows increase in the percentage of FOXA2+ cells after treatment with AA
806 and (g) induction of NKX2-1 and PAX8 after Dox treatment (day 9). qRT-PCR analysis for
807 exogenous and endogenous *NKX2-1* and *PAX8*, *FOXE1*, *TG* and *TSHR* after Dox stimulation.
808 (i) Gene expression curve of *TG* and exogenous *NKX2-1* and *PAX8* from day 9 to day 16 of the
809 differentiation protocol. Unpaired t-test and Kruskal-Wallis test Multiple comparisons were
810 used for statistical analysis. All analysis were performed using at least three independent
811 experiments. **$p<0.01$, ***$p<0.001$. Scale bars, 50 μm.
812

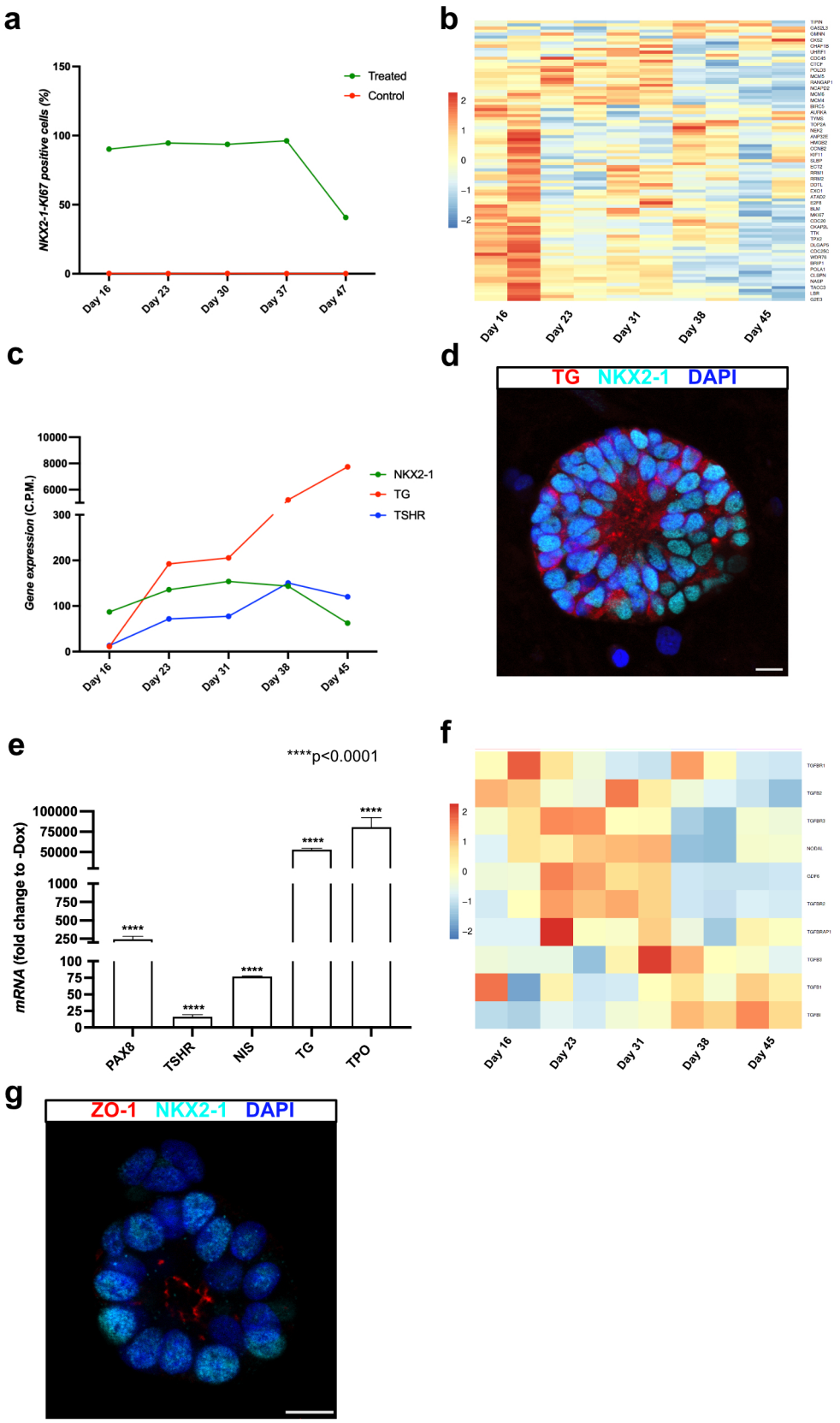

Extended data Fig. 2. Characterization of the proliferation and early differentiation stages of the human thyroid protocol. (a) Proportion of NKX2-1^{GFP+} cells expressing the

816 proliferation marker KI67 during the differentiation protocol. (b) Heatmap of bulk RNA-Seq
817 expression of proliferation markers in NKX2-1^{GFP+} cells at different stages of the
818 differentiation protocol. Rows represent the marker and columns the specific time point. Color
819 values represent mean expression levels. (c) *NKX2-1*, *TG* and *TSHR* gene expression curve
820 (bulk RNA-Seq data) at different stages of the protocol. (d) NKX2-1 and TG co-staining, at
821 day 28, showed progressive follicular organization, without the monolayer epithelium, but with
822 the appearance of the luminal compartment. (e) qRT-PCR analysis of *PAX8*, *TSHR*, *NIS*
823 /*SLC5A5*, *TG* and *TPO* genes at day 45 compared to -Dox control. (f) Heatmap of bulk RNA-
824 Seq expression of TGFβ signaling markers within NKX2-1^{GFP+} cells by differentiation
825 protocol. (g) NKX2-1 and ZO-1 co-staining, at day 45, shows the single-layered thyroid
826 follicular epithelium and the delimited lumen formed. An unpaired t-test was used for statistical
827 analysis and three independent samples were used for analysis. ****$p<0.0001$. Scale bars, 10
828 μm.
829

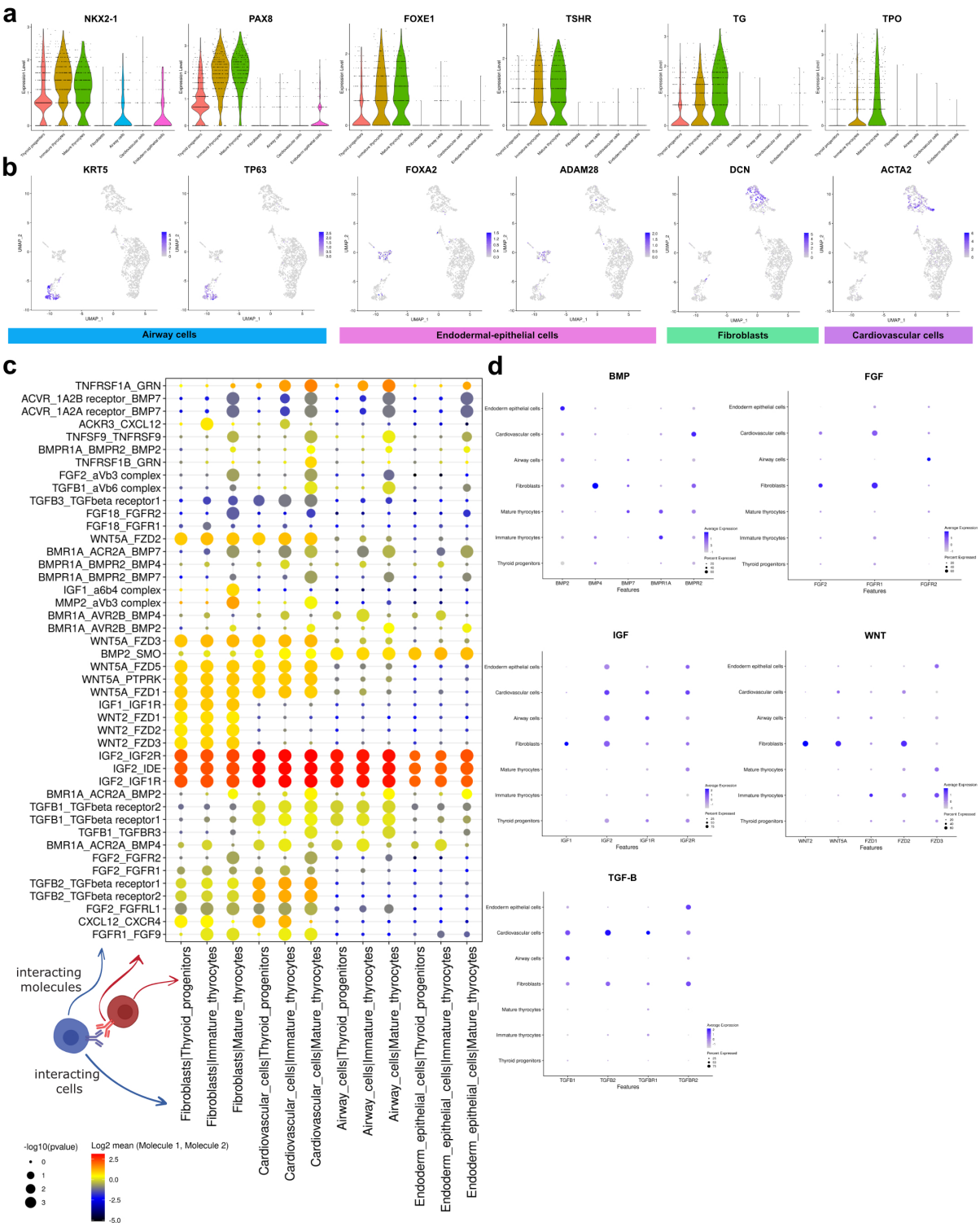

Extended data Fig. 3. scRNA-Seq clusters characterization and CellPhone-DB heterotypic interaction between thyroid populations and other cells. (a) Violin plots showing expression levels of key thyroid markers between thyroid clusters and other cells. (b) UMAP plots showing the expression of specific differentially expressed markers for non-

835 thyroidal clusters. (c) Diagram showing selected ligand-receptor interactions using
836 CellPhoneDB on the single-cell dataset of human thyroid organoids; P values are indicated by
837 circle size. The color scale shows the Log2 mean values of the average expression level of
838 interacting molecule 1 from cluster 1 and interacting molecule 2 from cluster 2. (d) Dot plot
839 visualization of markers expression from selected relevant interactions data across clusters.
840 Shown are the expression levels of receptors and ligands for BMP, FGF, IGF, WNT and TGFβ
841 pathways. The size of the circles indicates the percentage of expression. The color scale bar
842 indicates the mean values of the average expression levels.
843

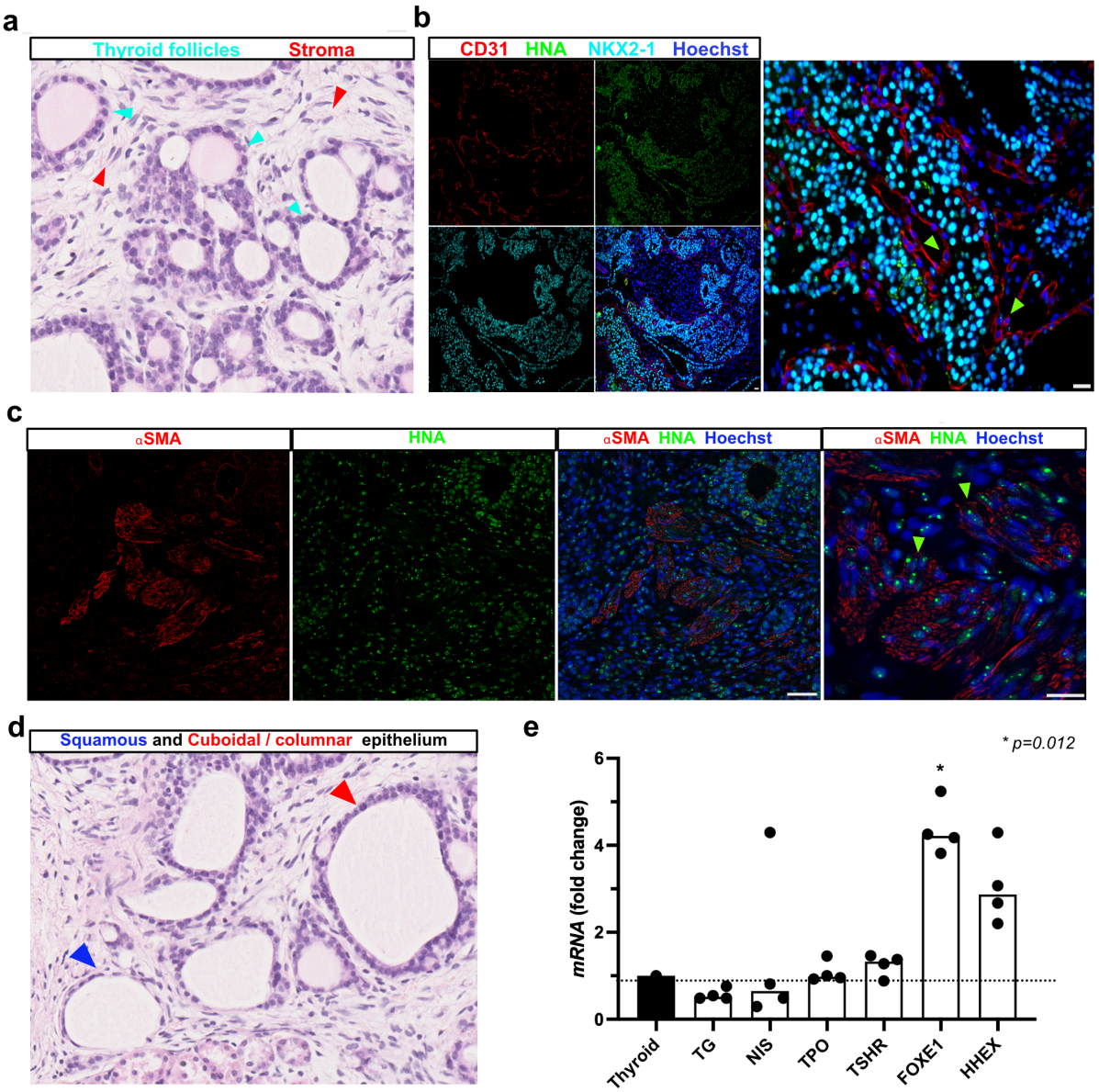

Extended data Fig. 4. Histological characterization of transplanted human thyroid tissue. (a) H&E staining shows the presence of multiple thyroid follicles (green arrows) surrounded by stromal cells (red arrows). (b) NKX2-1 and CD31 immunostaining demonstrate the presence of a dense network of small blood vessels in close proximity to the thyroid follicles. CD31+ cells do not express HNA (green arrows), providing clear evidence that the endothelial cells are host-derived. (c) Co-staining of a-SMA and HNA (green arrows) indicates a human origin of the stromal cells. (d) Histological analysis shows the presence of active follicles with cuboidal to weakly columnar epithelium (red arrows) and inactive follicles with flat/scaly cell

853 organization (blue arrows). (e) Gene expression levels of thyroid markers in transplanted tissue

854 (n=4) compared to human thyroid tissue. An unpaired t-test was used for statistical analysis.

855 *p<0.012. Scale bars, 20 µm.

856

857 **Tables**

858

859 **Extended table 1: Human differentiation medium composition**

860

hESC Differentiation Medium	**Stock concentration**	**Final concentration**	**Volume (50 ml)**
DMEM/F12 + Glutamax			38.4 ml
FBS		20% v/v	10 ml
MEM-Non-Essential Amino Acids (MEM-NEAA)	100x	1%	500 µl
Sodium pyruvate	100x	1%	500 µl
P/S	100x	1%	500 µl
2-Mercaptoethanol (in PBS)	7%	0.007%	50 µl
Vitamin C	50 mg/ml		50 µl

861

862 **Extended table 2:** List of primary and secondary antibodies used in the experiments.

Primary antibodies					
Protein Target	***Provider***	***Catalog number***	***Host Species***	***Dilution Flow Cyt.***	***Dilution IF***
AFP	Santa Cruz	sc-8108	Goat		1:100
β-III Tubulin	Eurogentec	MMS-435P-200	Mouse		1:1,000
αSMA	Abcam	ab32575	Rabbit		1:1,000
NKX2-1	Abcam	ab76013	Rabbit		1:500
PAX8	Cell Signaling	59019	Rabbit		1:500
TG	Dako	A0251	Rabbit		1:2,000
TG	Abcam	Ab187378	Mouse		1:250

TPO	Santa Cruz	sc-58432	Mouse		1:100
T4	Biorbyt	orb11479	Goat		1:1,000
T4	Invitrogen	MA5-14716	Mouse		1:100
E-cadherin	BD	610181	Mouse		1:1,000
CD31	R&D	AF3628	Goat		1:100
HNA	Abcam	ab190710	Mouse		1:250
KI67	Abcam	ab15580	Rabbit	1:100	
Secondary antibodies					
Cy3-conjugated	Jackson Immunoresearch	715-165-150	Donkey anti-mouse IgG		1:500
Cy3-conjugated	Jackson Immunoresearch	711-165-152	Donkey anti-rabbit IgG		1:500
Cy3-conjugated	Jackson Immunoresearch	705-165-147	Donkey anti-goat IgG		1:500
Alexa fluor 488-conjugated	Jackson Immunoresearch	715-545-150	Donkey anti-mouse IgG		1:500
Alexa fluor 647-conjugated	Jackson Immunoresearch	715-605-150	Donkey anti-mouse IgG		1:500
Alexa fluor 647-conjugated	Jackson Immunoresearch	711-605-152	Donkey anti-rabbit IgG	1:300	1:500

863

864 **Extended table 3:** List of primers sequences used for qRT-PCR analysis.

Gene name	Primer Forward	Primer Reverse
FOXA2	GGGAGCGGTGAAGATGGA	TCATGTTGCTCACGGAGGAGTA
SOX17	GTGGACCGCACGGAATTTG	CACGTCAGGATAGTTGCAGTAAT
exNXK2-1	TGTCCTGCTCCACCTTGCT	CGCACACCGGCCTTATTCCA
exPAX8	CCTCGGTGCACATGCTTTAC	GAGGTCTGCCATTCACAAAGG
NKX2-1	GCTTCCCCGCCATCTCC	GCCATGTTCTTGCTCAGCTC
PAX8	CGAGCGACTCCCCGGCGAT	GAGGTCTGCCATTCACAA
FOXE1	GCGACAACCCCAAAAAGTGG	GCCCAGTAGCCCTTACC
HHEX	GGACGGTGAACGACTACACGCA	CCAGACGCTTCCTCTCGGCGC
TG	AGACACCTCCTACCTCCCTCA	TCCTTGGACATCGCTTTGGC
TSHR	TGACCTTTCTTACCCAAGCCA	TGCTCTCAAGGACTTACACATCA

TPO	CTGTCACGCTGGTTATGGC	GCTAGAGACACGAGACTCCTCA
NIS/SLC5A5	ATCGCTATGGCCTCAAGTTCC	TCCAGGTACTCGTAGGTGCT
GAPDH	CTATAAATTGAGCCCGCAGCC	TACGACCAAATCCGTTGACTC

865